Bull. Soc. Photogr. Imag. Japan. (2018) Vol. 28 No. 2: 9–17

Original Papers

Ease-to-use approach of BRDF recovery from 360°Light Probe

Ryota Domon[(1)], Shoji Yamamoto[(2)], Hiroshi Kintou[(3)], Norimichi Tsumura[(1)]

Abstract: We present an easy-to-use measurement of BRDF for material appearance of three-dimensional object based on the estimation of surface reflectance properties with 360-degree light probe. Conventional methods of BRDF measurement such as gonio-reflectometry have some problems relating to the size, cost, and difficulty of operation. Appearance from Motion Method proposed by Dong et al. is appropriate to conquer above problems. Their method attempted to estimate the surface reflectance under unknown incident light component. However, a use of multiple unknown parameters causes the loss of convergence, and sometimes sacrifices the accuracy and computational cost. Therefore, we improved their algorithm of Appearance from Motion method by using an omni-directional camera as a light probe. We demonstrate valuable results: Higher reproducibility and lower cost of computation than those of the conventional method.

Key words: BRDF, Measurement, 360-degree light probe, Reproduction

1. Introduction

The important information of surface reflectance is useful for the field of computer graphics. This information is defined as bi-directional reflectance distribution function (BRDF) to calculate an appearance of object. Especially, since Spatially-Varying BRDF (SVBRDF) has information of spatially variation of the objects, therefore, SVBRDF is used for the rendering of virtual object with multiple textures. Various profile of this BRDF changes the material appearance based on dichromatic reflection model. Specular reflection represents the surface smoothness by its degree of reflection.

Conventionally, the use of BRDF information was limited in the field of computer science. Recent revolution of three-dimensional (3D) reproduction gives us the useful chance of BRDF information in commercial production. Actually, there are many applications of internet shopping, reproducing in digital mock-up, arts, and regenerative medicine. The most expected contribution of BRDF information is application for rapid proto-typing that is compatible to final product with same property of surface roughness. Therefore, the method of BRDF measurement attracts attention as the essential tool for advancement of 3D reproduction.

Various measurement methods have been proposed for the accurate BRDF of real object. However, the currently used method or instruments such as gonio-reflectometer has large scale, needs high calculation cost and difficult to acquire BRDF information. Moreover, it is difficult for non-expert user to measure the appearance of the object. For this reasons, the measurement system, which is commercially available, rapid and compact, is required for handling the appearance.

In this paper, therefore, we propose a rapid and compact measurement system that is expected to be equipped with 3D reproduction system. Our method refers to Appearance from Motion method proposed by Dong et al.[1)], whereas we make a goal to ascend the industrial value by adding an extra procedure which is the use of environment map captured by omni-directional camera instead of the estimation of an incident lighting component. This improvement provides the accuracy and simplification compared with the conventional method.

2. Related Work

Appearance reproduction is well-studied with BRDF, which is physical model for representing photon propagation. There are many kinds of appearance measurement method or instruments as previous works [2)-5)]. In general, the recovery of object appearance needs three information, such as geometry (normal vector), surface reflectance (BRDF), and incident lighting component [6)]. When the shape of object is assumed as a flat plate to fix the geometrical parameter, the gonio-reflectometer can be useful to acquiring the BRDF parameters for reproduction of various appearances. Unfortunately, accurate BRDF measurement needs 6 DOF movement and precious position arrangement. Therefore, a tangled repeat setting and long measurement time are required. In order to decrease the time and effort, multiple lighting or wide view camera system was proposed to detect much reflectance information at one shot [7)-14)]. Although these ideas can reduce the measurement cost dramatically, the flexibility of the BRDF measurement was lost by reason of fixed and limited measurement equipment.

A breakthrough idea for this complicated BRDF measurement was proposed by Dong et al. in ACM SIGGRAPH Asia 2014 [1)].

Received 25th April, 2018; Accepted 6th October, 2018

[(1)]Graduate School of Advanced Integration Science, Chiba University, CHIBA, JAPAN
[(2)]Tokyo Metropolitan College of Industrial Technology, TOKYO, JAPAN
[(3)]Nikon Corporation, TOKYO, JAPAN

Their method can reconstruct the BRDF information at spatially varying isotropic surface (SVBRDF) by solving ill-posed problem between the reflectance and illumination without the knowledge of incident light. Only capturing the video while rotating the objects, non-expert users are also accessible and easy to control, because acquisition scheme of this method is greatly simplified. In this method, they estimated three unknown variables; distribution of specular highlights, diffuse albedo, and lighting component, under the condition that the shape of object is known. Moreover, their group expanded their method to estimate the shape information with the estimation of reflectance and illumination by using the temporal trace processing from the measured data [15].

Although it is arguable for the estimation of all information since the measurement technology for 3D shape is remarkably developed [16], their state-of-the-art method is undeniably useful for the reconstruction of object appearance. This method proposed by Dong et al. was based on the attempt to set various restrictions to solve this complex problem and demonstrated feasible result of acquiring the surface reflectance. However, the estimation of several variables such as albedo, specular, and illumination in their method causes less convergence and more computational cost. Moreover, lighting component calculated by their method indicated uncertain artifacts in the result of their estimation. For example, the edge of estimated lighting components are affected by target object or immoderately saturated in Fig. 17 of SIGGRAPH paper, since their method converges their calculation when the edge of illumination was sharpened. Here, it is noticed that the estimation of lighting component will have an insignificant importance because incident lighting is easy to measure by using omni-directional cameras that become compact and low price. Therefore, we improve and simplify the Dong's method for the guarantee of convergence and rapid estimation under known lighting condition, which is derived environmental image captured by omni-directional cameras.

3. Method

3.1 Acquisition and Calibration

Our proposed method requires the measured images of object that is rotating on the table, environmental image to provide an incident lights on the target object, and geometry data of target object. We captured images of object on the rotating table by digital camera (D5100, Nikon) equipped with varifocal lens (AF-S NIKKOR 24-120mm, Nikon) as shown in Fig.1. Intrinsic camera parameters were precomputed by using the method of Zhang et al. [17] and the captured image was saved every one degree of rotating angle as a radiometrically linear RAW image with single exposure. Environmental image as the 360-degree light probe was also captured by omni-directional camera (Theta, Ricoh). In order to use this image captured with omni-directional camera as the incident light component, it is necessary to consider the radiometrically linearity and color matching with digital camera. To solve this problem, we reproduced high dynamic range (HDR) image by capturing 11 images with different exposure time. HDR composition was carried out with the method proposed by Debevec et al. [18]. After that, we used Munsell color chart for linear correction and performed the color matching between digital camera and omni-directional camera. Through these processing, we derived incident light component from omni-directional camera as shown in Fig.2. The feature of object was measured in sequence by using a rotational stage (SGSP-60YAW, Sigma-Koki). In this experiment, we prepared real object which was simple plate or cylinder as the measurement target. Since the shape of these objects is fully axisymmentrical, we also prepared the polygon model based on the measured data with real size of each object. The polygon model was registered to the first frame of image sequences by hand with GUI application. Here, it is noted that the subsequent frames are automatically registered between real object and its polygon data, because the rotational position of each frames are known and the center of rotation is consistent.

3.2 Assumption and input data

Our proposed method refers to the pioneering idea proposed by Dong et al.[1] We assume that surface reflectance is isotropic and it is expressed by microfacet reflectance model. As the dichromatic BRDF model is used in our system, the surface reflectance at a point x is defined by Eq.1.

$$f(\boldsymbol{\omega}_i, \boldsymbol{\omega}_o; x) = \frac{\rho_d(x)}{\pi} + \rho_s(x) f_s(\boldsymbol{\omega}_i, \boldsymbol{\omega}_o; x) \quad (1),$$

where ω_i and ω_o are the incident and reflected directions, ρ_d and ρ_s are the diffuse and specular reflectance, and $f_s(\omega_i, \omega_o; x)$ is the specular reflectance function, which is proposed by Asikhmin et

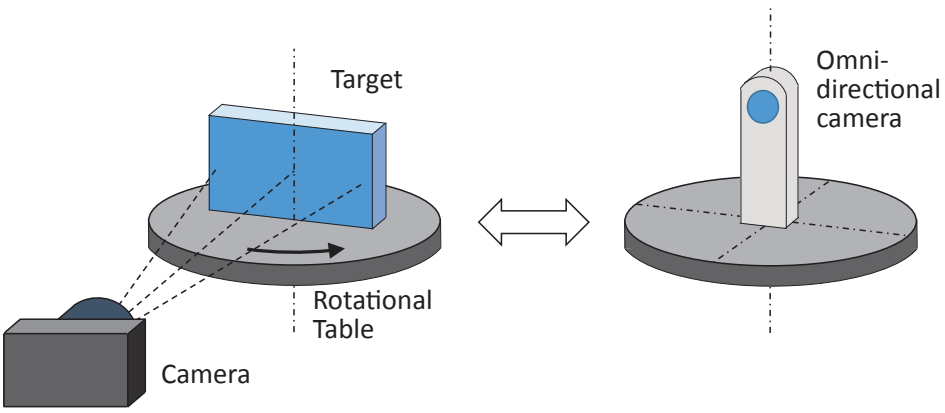

Figure 1 Illustration of our experimental setup for BRDF measurement and incident light capturing by 360-degree omni-directional camera.

Figure 2 Example of light probe which is HDR image captured by 360-degree omni-directional camera.

al. as follows [19] .

$$f_s(\boldsymbol{\omega}_i, \boldsymbol{\omega}_o) = \frac{D(\boldsymbol{\omega}_h)G(\boldsymbol{\omega}_i, \boldsymbol{\omega}_o)F(\boldsymbol{\omega}_i, \boldsymbol{\omega}_o)}{4(\mathbf{i}\cdot\mathbf{n})(\mathbf{o}\cdot\mathbf{n})} \quad (2),$$

where $D(\omega_h)$ indicates the normal distribution function (NDF) of the halfway direction ω_h with microfacet, $F(\omega_i, \omega_o)$ indicates Fresnel reflectance function (we assumed a fixed index of refraction of 1.3 for all materials as same as Dong et al.) , and $G(\omega_i, \omega_o)$ indicates the shadowing and masking function. Because specular highlights are quite effective factor for appearance reproduction, it is very important to select the spatial distribution of specular highlights, namely NDF. We observed two major trends of spatial distribution of highlights in real world. Ceramic plates have weak tail in highlights as shown in Fig.3 (a). On the other hands, wooden flooring plate has relatively strong tail in highlights as shown in Fig.3 (b). Therefore, we employed two NDFs owing to represent these characteristics. First, we adopt Beckmann distribution model to express the weak tail in highlight as shown in Fig.3 (a). In other case, GGX model is adopted to express the strong tail in highlight as shown in Fig.3 (b) [20]. These models determine the spatial distribution by the angles between halfway direction ω_h and surface normal. For the simplification of acquiring the surface reflectance properties, we seek the roughness parameters of each model as the objective function instead of the 1-dimensional tabulated function that monotonically decreased used in previous study.

By solving the minimization problem, it is possible to obtain an appropriate value (surface reflectance properties) with residual simultaneously. It can be regarded as the smaller residual is suitable for representing the surface reflectance properties. For the reduction of computational cost, we employed Smith's shadowing and masking term, which has relatively less computation cost. In our method, three variables for each surface point are determined separately. To derive these parameters, we solve minimization problem denoted by Eq.3,

$$\underset{(\rho_d,\rho_s,D)_x}{\arg\min} \sum_t \sum_x \| I(\boldsymbol{\omega}'_o, x, t) - L(\boldsymbol{\omega}'_o, x, t) \|^2 \quad (3),$$

where $I(\omega'_o, x, t)$ is the observation value of rotating target object, $L(\omega'_o, x, t)$ is the outgoing radiance at a surface point x at time t. ω'_o indicates the outgoing (viewpoint) vector, and prime symbol is the direction in global coordinate. $L(\omega'_o, x, t)$ is determined by registered object geometry n(x,t) and incident light component $E(\omega'_i)$ captured with omni-directional camera as denoted in Eq.4.

$$L(\boldsymbol{\omega}'_o, x, t) = \int_\Omega f_r(\boldsymbol{\omega}_i(x,t), \boldsymbol{\omega}_o(x,t); x) E(\boldsymbol{\omega}'_i)(\mathbf{n}(x,t)\cdot\boldsymbol{\omega}'_i) d\boldsymbol{\omega}'_i \quad (4),$$

where ω_i and n indicates the lighting vector and surface normal at the surface point x. ω_i is the sampling area from environmental map captured by omni-directional camera. Based on the prior work, we set the range of sampling area less than 0.5π from the mirror reflection with respect to the viewpoint vector. This idea is very simple but it is effective to reduce the computational cost. Figure 4 shows the illustration of acquiring incident light component from

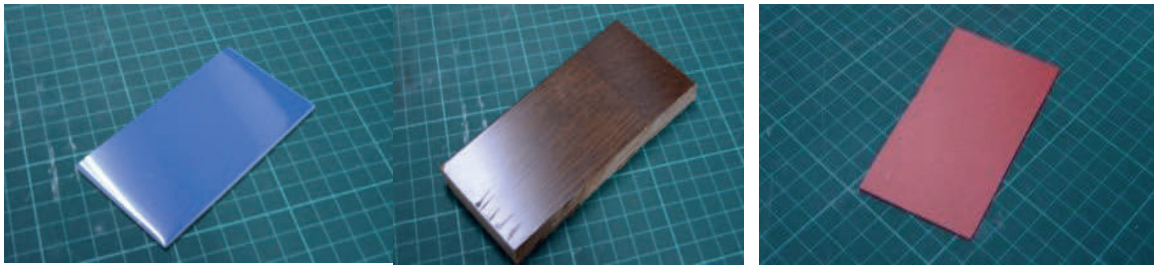

(a) (b) (c)

Figure 3 Various spatial distribution of highlights in real world material, (a) Ceramic plate, (b) Wooden flooring plate, (c) Red gum plate.

the environmental map which is captured with omni-directional camera.

3.3 NDF Recovery

Our proposed method solves Eq.3 with each surface point separately. Thus, we rewrite Eq.3 to denote the equation of a single surface point x,

$$\arg\min_{(\rho_x,\rho_s,D)_x} \sum_t \| T(\boldsymbol{\omega}'_o,t) - L(\boldsymbol{\omega}'_o,t) \|^2 \tag{5},$$

where $T(\omega'_o, t)$ is equal to $I(\omega'_o, x, t)$, which represents the temporal variation at the surface point x as shown in Fig.5. It is difficult to solve Eq.5 because there are still three variables. Therefore, we take temporal gradient of observation and outgoing radiance on the surface point x. Temporal gradient of the outgoing radiance can be expressed as Eq.6.

$$\begin{aligned}\nabla_t L(\boldsymbol{\omega}_o,t) &= \nabla \int_\Omega f_r(\boldsymbol{\omega}_{ix}(t),\boldsymbol{\omega}_{ox}(t))E(\boldsymbol{\omega}'_i)(\mathbf{n}_x(t)\cdot\boldsymbol{\omega}'_i)d\boldsymbol{\omega}'_i \\ &= \nabla_t \int_\Omega \frac{\rho_{dx}}{\pi} E(\boldsymbol{\omega}'_i)(\mathbf{n}_x(t)\cdot\boldsymbol{\omega}'_i)d\boldsymbol{\omega}'_i \\ &+ \nabla_t \int_\Omega \rho_{sx} f_{sx}(\boldsymbol{\omega}_{ix}(t),\boldsymbol{\omega}_{ox}(t))E(\boldsymbol{\omega}'_i)(\mathbf{n}_x(t)\cdot\boldsymbol{\omega}'_i)d\boldsymbol{\omega}'_i \\ &= \frac{\rho_{dx}}{\pi}\nabla_t \int_\Omega E(\boldsymbol{\omega}'_i)(\mathbf{n}_x(t)\cdot\boldsymbol{\omega}'_i)d\boldsymbol{\omega}'_i \\ &+ \rho_{sx}\nabla_t \int_\Omega f_{sx}(\boldsymbol{\omega}_{ix}(t),\boldsymbol{\omega}_{ox}(t))E(R_{nx(t)}(\boldsymbol{\omega}_i))\boldsymbol{\omega}_{iz}d\boldsymbol{\omega}'_i \end{aligned} \tag{6}.$$

There are two terms in Eq.6, diffuse reflection component and specular reflection component. Because temporal variation of diffuse component is comparatively small, temporal gradient of the diffuse component can be assumed approximately zero. Hence, specular component, which is principally effected by lighting, is the dominant factor of outgoing radiance denoted as Eq.7.

$$L(\boldsymbol{\omega}'_o,x,t) \approx \rho_s(x)\int_\Omega f_{sx}(\boldsymbol{\omega}_i,\boldsymbol{\omega}_o(t))\boldsymbol{\omega}_{iz}E(R_{nx(t)}(\boldsymbol{\omega}_i))d\boldsymbol{\omega}'_i \tag{7}.$$

Taking that approximation, we can simply solve the minimization problem denoted in Eq.8 with temporal gradient of the observation and outgoing radiance denoted in Eq.7.

$$\arg\min_{D'_x} \sum_t \| \nabla_t T(\boldsymbol{\omega}'_o,t) - \int_\Omega f_{sx}(\boldsymbol{\omega}_i,\boldsymbol{\omega}_o(t))\boldsymbol{\omega}_{iz}E(R_{nx(t)}(\boldsymbol{\omega}_i))d\boldsymbol{\omega}' \|^2 \tag{8},$$

where $D'x$ is the unnormalized NDF biased by specular albedo ρ_{sx}. Finally, the NDF Dx is recovered from $D'x$ via unit integration. In our implementation, we employ two NDFs, Beckmann distribution and GGX distribution. It is expected that residual of minimization problem may be reduced if the characteristics of NDF is suitable for representing the surface reflectance of target object. We adopt the result which has smaller residual value for verifying the accuracy of our proposed method.

3.4 Albedo Recovery

Given the recovered NDF D_x from previous formulation, we can now determine the diffuse component and specular component of outgoing radiance denoted as Eq.9.

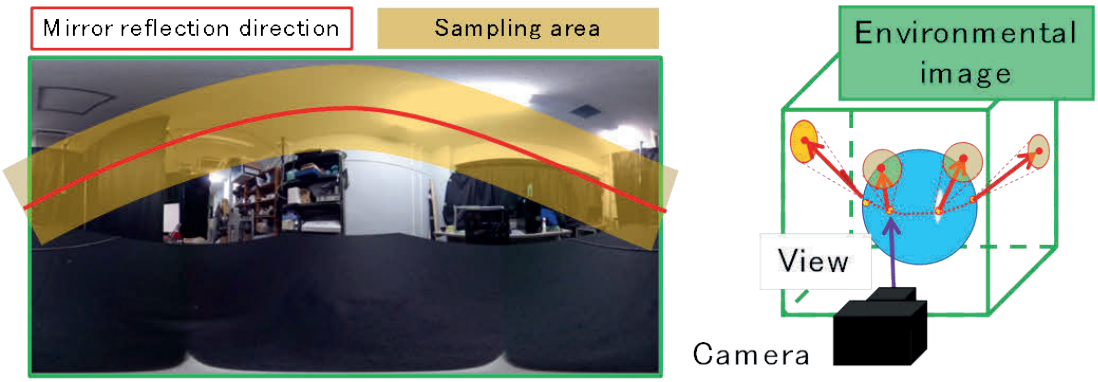

Figure 4 Illustration of acquiring incident light component from the HDR image captured with omni-directional camera.

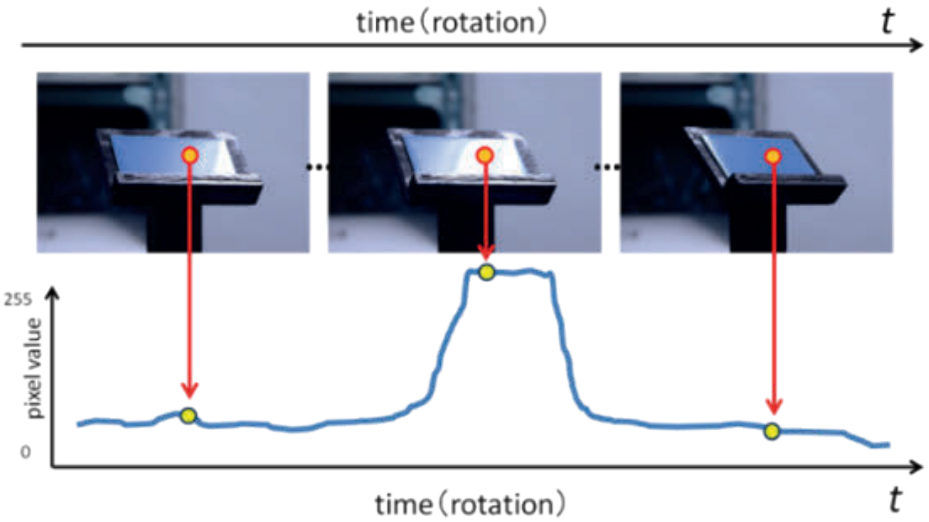

Figure 5 Temporal variation of pixel value during the measurement with a rotational table.

$$
\begin{aligned}
T_{dx}(\boldsymbol{\omega}_o, t) &= \int_\Omega f_r(\boldsymbol{\omega}_{ix}(t), \boldsymbol{\omega}_{ox}(t)) E(\boldsymbol{\omega}_i')(\mathbf{n}_x(t) \cdot \boldsymbol{\omega}_i') d\boldsymbol{\omega}_i' \\
&= \frac{\rho_{dx}}{\pi} \int_\Omega E(\boldsymbol{\omega}_i')(\mathbf{n}_x(t) \cdot \boldsymbol{\omega}_i') d\boldsymbol{\omega}_i' \\
&+ \rho_{sx} \int_\Omega f_{sx}(\boldsymbol{\omega}_{ix}, \boldsymbol{\omega}_{ox}) E(\boldsymbol{\omega}_i')(\mathbf{n}_x(t) \cdot \boldsymbol{\omega}_i') d\boldsymbol{\omega}_i' \\
&= \rho_{dx} T_{dx}(\boldsymbol{\omega}_o', t) + \rho_{sx} T_{sx}(\boldsymbol{\omega}_o', t)
\end{aligned} \tag{9}
$$

$T_{dx}(\omega_o, t)$ and $T_{sx}(\omega_o, t)$ are diffuse trace and specular trace of the outgoing radiance. It can be regarded that the observation trace $T(\omega_o', t)$ is the weighed sum of normalized diffuse trace and specular trace. As a result, recovery of the albedo components are formulated as non-negative least squares minimization problem as shown in Eq.10.

$$
\arg\min_{(\rho_d, \rho_s)_x} \sum_t \| T_x(\boldsymbol{\omega}_o', t) - (\rho_{dx} T_{dx}(\boldsymbol{\omega}_o', t) + \rho_{sx} T_{sx}(\boldsymbol{\omega}_o', t)) \|^2 \tag{10}
$$

4. Verification

4.1 Evaluation for estimated BRDF

In order to validate our proposed method, we prepare synthetic image generated by Mitsuba renderer [21]. We rendered three kinds of objects by changing surface reflectance as shown in upper row of Fig.6. These images rendered with the office window environment map (Fig.2) and used Beckmann distribution, and lower row images were rendered by using the acquired surface reflectance from our proposed method. Comparing upper to lower images, it can be confirmed that the calculated surface reflectance properties can make a reasonable image with our proposed method. Though the calculated parameters of the most right one in upper and lower row are different, visual difference is slightly small.

We also evaluated the validity of our proposed method by comparing with the NDF acquired by gonio-reflectometer (GCMS-4, Murakami Color Research Laboratory). To measure the surface reflectance of the objects, we take three type of flat board objects, blue ceramic, wooden flooring plate and red gum (Also shown in Fig.3) . Figure 7 shows the results of measurement by using gonio-reflectometer and our proposed method, where blue line in the Fig.6 is measured by gonio-reflectometer, and red line and green line in Fig.7 are Beckmann distribution model and GGX distribution model, respectively. As we expected, surface reflectance of each target object is recovered by appropriate NDF to represent each material. Figure 8 shows the reproduced image by using acquired NDF value. It is apparent that NDFs of each of the subjects are estimated accurately as same as the gonio-reflectometer and rendered images of appearance is observed as a quite similar to original board objects.

4.2 Evaluation for SVBRDF measurement

Next, we challenged to reproduce the SVBRDF profile which is set up in the surface of aluminum can with multiple texture. Figure 9 shows the picture of real object (left) and measured result of diffuse albedo map (right) by using our system. From the result, our system can obtain the meaningful albedo map which can recognize as a combination of different textures. It can distinguish each texture and positional relationship, unfortunately, it is hard to make reasonable result for measurement of SVBRDF. This result indicates that our measurement system has some incompleteness and improvement for SVBRDF measurement. For its causes and solutions, we will describe in the latter discussion part in this paper.

4.3 Subjective appearance evaluation

In this section, we verified the BRDF recovery by using real 3D objects, which has distinctive surface appearance. Four types of 3D object with different surface profile were selected, such as green gum ball, urethane coated bowl, white ceramic vase and blue plastic cone. Figure 10 shows the results of this verification under the same condition and measurement instrument as Fig.7. The left side image in Fig.8 shows real objects, and right side image shows rendered ob-

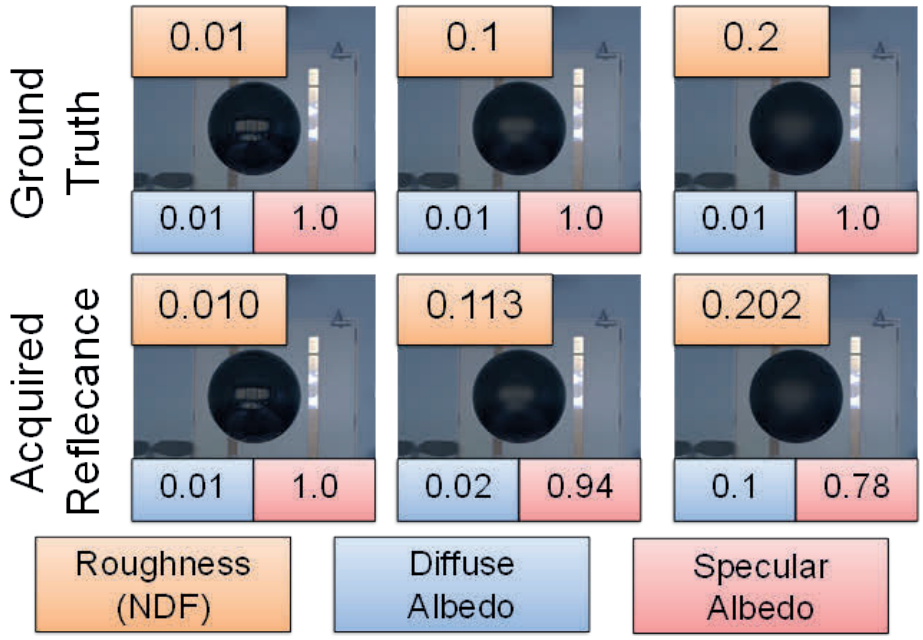

Figure 6 Results of synthetic image generated by Mitsuba renderer based on the calculated three variables, which are roughness, diffuse albedo, and specular albedo. Each numerical value indicates the comparison between measured ground truth and calculated result by using our method.

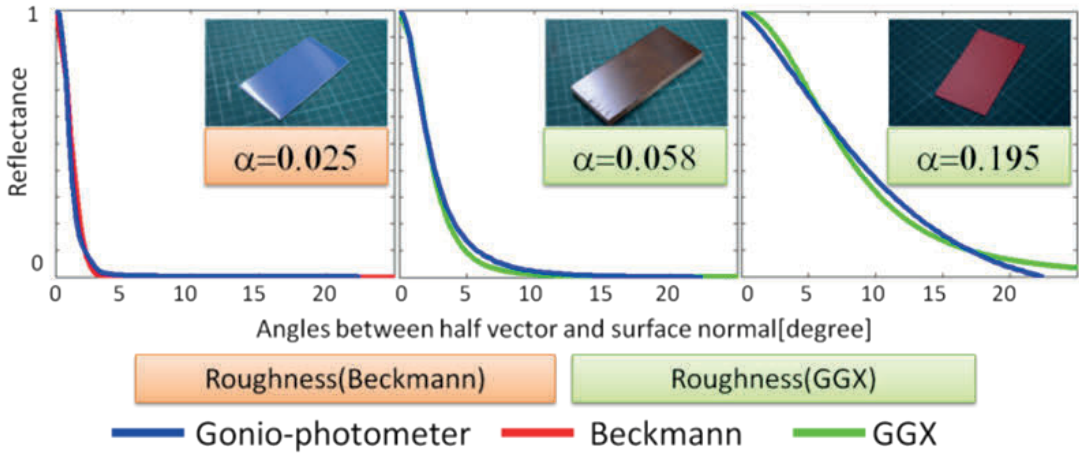

Figure 7 Comparison results of reflectance distribution between our proposed method and gonio-reflectometer.

Figure 8 Reproduced images by using acquired NDF value. (a) Blue ceramic plate, (b) Wooden flooring plate, (c) Red gum plate.

Figure 9 Result of SVBRDF measurement by using aluminum can with multiple texture, (a) Real object, (b) diffuse albedo map.

jects by using Mitsuba renderer with Reinhard's tone mapping operator [22]. The calculation for matching the distribution model was performed by using the Beckman and GGX models, and we selected the best matching model between estimated and modeled reflectance.

Here, it is noted that we have no choice but to evaluate the appearance by appreciation since it is difficult to acquire the ground truth of these 3D object. Therefore, we applied subjective evaluation to verify each rendering result. The color corrected display (CX241-CNX, EIZO) was used, and fifteen participants with normal color vision assessed by using five grade evaluation, (5:quite similar, 4:rather similar, 3:similar, 2:rather not similar, 1: not similar). Figure 11 shows the result of histogram for five grade in this subjective evaluation.

As a comprehensive evaluation, our proposed method is possible to measure and reproduce the surface appearance of material even if the target is 3D object. The highest score was granted for the result of white ceramic vase. From the participant's comment, a clear surface reflectance of specular represents the appearance of ceramic material gradely. On the other hand, the reproduction of blue plastic cone had the lowest score, since the contrast between specular and diffuse color was ill-balanced in comparison to real 3D object. Commonly, it is difficult to use the best tone mapping in changing from 32bit to 8bit signals because the measured BRDF is expressed by high dynamic range data. In this experiment, we made the visual appearance close to real object by controlling the exposure of omni-directional images. However, a slight difference of tone balance

provides an unpleasant impression in rendering reproduction such as the case of blue plastic cone and green gum ball. The other results of urethane coated bowl was satisfied by almost participants. They appreciated the matching of specular distribution on the surface of 3D object, although ill-balanced contrast between specular and diffuse color is slightly concerned. Therefore, for visual verification, the consideration for model matching is necessary to attach importance as either specular or diffuse reflectance. In our case, the colored object should be attached importance to the diffuse reflection and monotone object should be attached importance to the specular reflection.

5. Discussion

5.1 Measurement setting and SVBRDF recovery

In this paper, it is blindingly clear that our proposed system can measure accurate BRDF when the target object consists of unique material. For this result, we infer that position-independent and integrated best solution is obtained by the calculation in an optimized process. On the other hand, more rigid measurement about position matching is required for the SVBRDF measurement, since the BRDF profiles are changed according to the measurement position. Therefore, all of the geometries in our work are formulated by combination of simple geometries, such as a sphere, cuboid, cylinder and so on. Moreover, many number of trial for position alignment were executed for the SVBRDF measurement, although this alignment was performed manually. However, this result indicates that our measurement system has some incompleteness.

From the result as shown in Fig.9, we can observe several unnatural features which are related to the position misalignment. At first, we notice a blurred edge at the part of trade name into the rotated direction. Moreover, we found that the detail part of "d" or "u" character have a serious blur compared with the first character "R". This unnatural result of blur leads us to some assumptions that the rotated table is hard to keep accurate one degree of angle, the center of object is out of alignment from the rotated center, and the shape of real object is partly distorted compared with polygon geometry. It is obvious that the blur image is generated as the mixture of diffuse albedo and specular reflection since the BRDF at misaligned point is estimated by using the different normal vector. In order to decrease the mixture of diffuse and specular reflection, the use of polarizer may be appropriate [4]. Unfortunately, this workaround idea invites an additional measurement in order to change the direction of

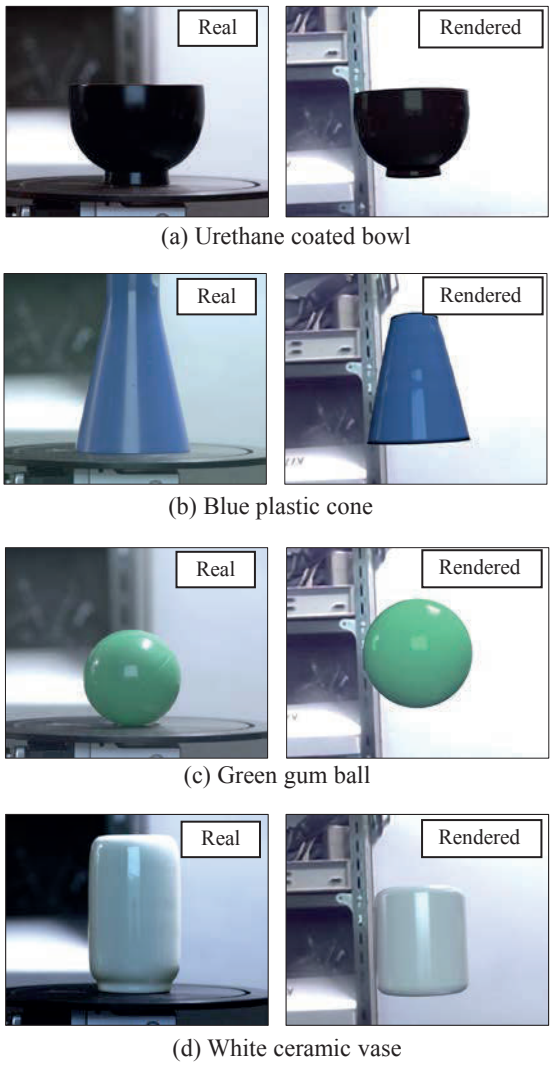

Figure 10 Images for subjective evaluation. The Left images show the captured image of 3D real objects, and the right images show the rendered results by our proposed method.

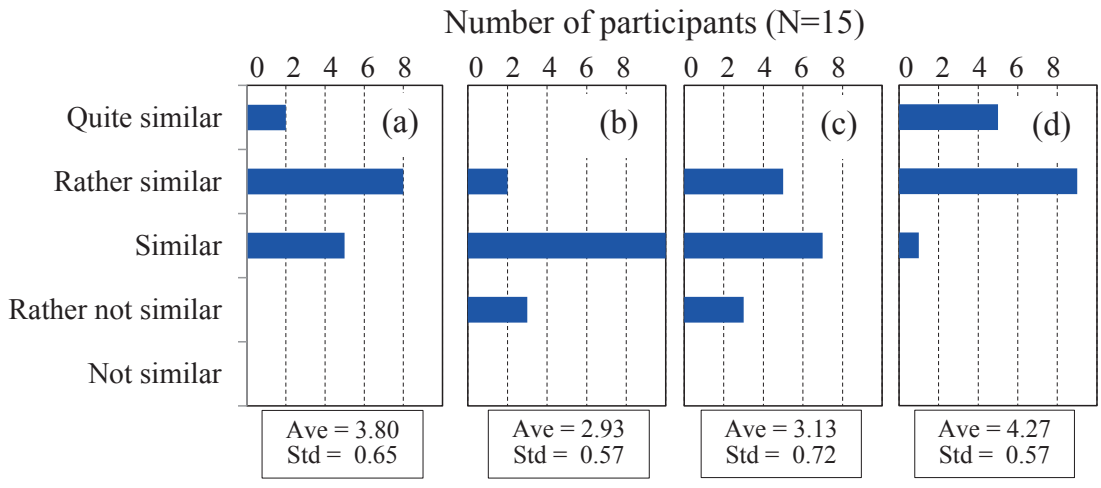

Figure 11 Result of subjective evaluation for our rendered images.

polarization, and more than all, the user always should prepare the polarizer every time.

Other unnatural feature in Fig.9 is found that the irregularity of up and down is existed in the horizontal linear edge. This misalignment infers that the slight movement of up and down side may be generated every movement by the rotating table. As just described, it is necessary to improve the precision of position alignment and stability of movement with careful consideration of requisite resolution in SVBRDF measurement. As an essential solution for this problem, it may be useful to measure the shape of object together by using digital camera. However, it might bring the trade-off between an accuracy of SVBRDF and computational cost, since a complicate and corrective calculation is necessary to measure the shape of object which has specular reflection on its surface. Recent novel instrument of 3D measurement may be possible to obtain the accurate shape even if target has the specular reflection [16]. Unfortunately, it is necessary to match the position and shape between measured shape and measurement point of BRDF finally.

5.2 Calculation cost reduction

Another priority of our proposed method is reduction of computational cost. Since our proposed method uses environmental map as the incident light component, the computational cost is simply reduced. Not to require the estimation of incident light component, we can estimate each surface reflectance independently. This independence of calculation will provide several merits that the parallel computing technique is easy to apply for our proposed method, and it can accelerate estimation process dramatically. In order to confirm our superiority, we tried to compare the performance of calculation between conventional and our method. Unfortunately, it is only provided the fragmentary specification of computation and the concept of algorithm in Dong's paper. Therefore, we make two kinds of hypothetical comparison; one is clock speed competition and the other is simulation for each algorithm. Table 1 shows that the comparison of clock speed of ours and conventional methods. Clock speed of conventional method is calculated by their paper. Our implementation environment uses Intel Corei7 processor with 16 GB memory. On the other hand, conventional method uses dual Intel Xeon E5-2690 processor with 64GB memory. Our computational specification is obviously less powerful than their condition, however we can achieve faster calculation for BRDF recovery.

For the simulation of each algorithm, we estimate the computational cost of both methods with the object as shown in Fig.7(a). With same polygon size of object, same measured pixel, and same optimization algorithm, both BRDF and environmental illumination map was estimated as the conventional method. On the other hand, only the BRDF was estimated by using our proposed method under the condition that the incident lighting component was known. As the result of simulation, our method achieves this process about 10 seconds, and conventional Dong's method is necessary to calculate about 101 seconds. As a conclusion, we can acquire precious BRDF value about ten times faster than conventional method.

6. Conclusion and future work

In this paper, we present a simple BRDF measurement method with well-convergence and rapid estimation by adding the lighting component derived from omni-directional camera. Our proposed method accomplished compatibility between accuracy and speed-up of calculation by using environmental image as light probe. The accuracy of our measurement was verified by comparing the surface reflectance between our system and gonio-reflectometer, and it is confirmed that the surface reflectance of flat board objects is almost completely reproduced by appropriate NDF with fitting to the Beckmann and GGX distribution model. The accuracy of visual reproduction is verified by comparing the appearance between real and reproduced 3D object, and it is confirmed that most of the participants selected their answers as "rather similar", or "similar" in the subjective evaluation. Moreover, our proposed method achieves the speed ten times faster than that of conventional method owing to the simplification of incident light components.

Geometric data selection can also affect the result of both NDF and albedo recovery of SVBRDF. If the misalignment and variation between measuring point and shape position are existed, the image of reproduced surface texture becomes blurred. Therefore, it is necessary to take careful position alignment and stability of rotational movement for the acquisition of shape and reflection data. The misalignment and variation between measuring point and shape position make the image of reproduced surface texture blurred. Here, it is noted that they have a trade-off relationship both accuracy and calculation cost.

Comments by participants in the evaluation of our proposed method prompted us to evaluate the target object with more complex shape. Therefore, high density measurement of geometry data and precise position matching between 3D model and environmental image are necessary as a future work. Moreover, an appropriate control of HDR measured data should be developed for practical use of our method. The HDR measurement for light probe and object feature was embedded in proposed method. Therefore, a precise tone mapping for the visual reproduction of material appearance is also necessary as a future work.

Acknowledgments

This research was partially supported by the Ministry of Education, Science, Sports, and Culture, Japan Grant-in-Aid for Scientific Research of 24500267 and 15K00415, and Brain and Information Science on SHITSUKAN of 25135707.

Table 1 Result of comparison for computational speed between conventional and proposed method

Method	Maximum clock speed	Minimum clock speed
Dual Intel Xeon (Conventional)	396.8GFlops	6.2GFlops
Intel Core i7 (Ours)	53.28GFlops	13.2GFlops

References

1) Y. Dong, G. Chen, P. Peers, J. Zang, X. Tong, ACM Transactions on Graphics, **33** (6), Article No. 193, (2014).
2) W. Matusik, H. Pfister, M. Brand, L. McMillan, Proc. of Eurographics workshop on Rendering, pp. 241-247, (2003).
3) N. Alldrin, T. Zickler and D. Kriegman, IEEE conference on computer vision and pattern recognition, DOI: 10.1109/CVPR.2008.4587656, (2008).
4) A. Ghosh, T. Chen, P Peers, C. A. Wilson and P. Debevec, ACM Transactions on Graphics, **29**(6), Article No. 162, (2010).
5) A. Ghosh, G. Fyffe, B. Tunwattanapong, J. Busch, X. Yu and P. Debevec, ACM Transactions on Graphics, **30**(6), Article No. 129, (2011).
6) D. Guarnera, G.C. Guarnera, A. Ghosh, C. Denk, M. Glencross, Computer Graphics Forum, **35**(2), pp.625-650, (2016).
7) M. Ben-Ezra, J. Wang, B. Wilburn, X. Li, L. Ma, IEEE conference on computer vision and pattern recognition, DOI:10.1109/CVPR.2008.4587766, (2008).
8) A. Gardner, C. Tchou, T, Hawkins and P. Debevec, ACM Transactions on Graphics, **22**(3), pp.749-758, (2003).
9) J. Wang, S. Zhao, X. Tong, J. Snyder and B. Guo, ACM Transactions on Graphics, **27**(3), Article No.41, (2008).
10) P. Ren, J. Wang, J. Snyder, J. Tong and B. Guo, ACM Transactions on Graphics, **30**(4), Article No. 45, (2011).
11) M. Holroyd, J. Lawrence, T. Zickler, ACM Transactions on Graphics, **29**(4), Article No.99, (2010).
12) Y. Dong, J. Snyder, X. Tong, J. Snyder, Y. Lan, M. Benezra, B. Guo, ACM Transactions on Graphics, **29**(4), Article No.98, (2010).
13) C. Schwartz, M. Weinmann, R. Ruiters, A. Zinke, R. Sarlette, R. Klein, ACM SIGGRAPH Asia Sketches, Article No.28, (2011).
14) M. Aittala, T. Weyrich, J. Lehtinen, ACM Transactions on Graphics, **32**(4), Article No.110, (2013).
15) R.Xia, Y. Dong, P. Peers, X. Tong, Proc. of ACM SIGGRAPH Asia, **35**, (2016).
16) M. Zollhoefer, P. Stotko, A. Görlitz, C. Theobalt, M. Nießner, R. Klein, A. Kolb, Computer Graphics Forum, **37**(2), (2018).
17) Z., Zhang, IEEE Trans., **22**(11), (2000).
18) P. Debevec, J. Malik, Proc. ACM SIGGRAPH, Article No.31, (2008).
19) A. Michael, P. Shirley, Journal of graphics tools, **5**(2), (2000).
20) B. Walter, S. R. Marschner, H. Li, K. E. Torrance, Proc. of Eurographics, pp.195-206, (2007).
21) Mitsuba Renderer, https://www.mitsuba-renderer.org/
22) E. Reinhard, M. Stark, P. Shirley, J. Ferwerda, ACM Transactions on Graphics, **21**(3), (2002).